INTERNATIONAL JOURNAL FOR NUMERICAL METHODS IN ENGINEERING
*Int. J. Numer. Meth. Engng* (2008)
Published online in Wiley InterScience (www.interscience.wiley.com). DOI: 10.1002/nme.2488

# Concurrently coupled atomistic and XFEM models for dislocations and cracks

Robert Gracie and Ted Belytschko*, †

*Department of Mechanical Engineering, Northwestern University, 2145 Sheridan Road, Evanston, IL 60208-3111, U.S.A.*

SUMMARY

A method for the modeling dislocations and cracks by atomistic/continuum models is described. The methodology combines the extended finite element method with the bridging domain method (BDM). The former is used to model crack surfaces and slip planes in the continuum, whereas the BDM is used to link the atomistic models with the continuum. The BDM is an overlapping domain decomposition method in which the atomistic and continuum energies are blended so that their contributions decay to their boundaries on the overlapping subdomain. Compatibility between the continua and atomistic domains is enforced by a continuous Lagrange multiplier field. The methodology allows for simulations with atomistic resolution near crack fronts and dislocation cores while retaining a continuum model in the remaining part of the domain and so a large reduction in the number of atoms is possible. It is applied to the modeling of cracks and dislocations in graphene sheets. Energies and energy distributions compare very well with direct numerical simulations by strictly atomistic models. Copyright © 2008 John Wiley & Sons, Ltd.

Received 6 September 2008; Accepted 17 September 2008

KEY WORDS: multiscale; bridging domain method; extended finite element method; dislocations; cracks

## 1. INTRODUCTION

Simulations with atomistic resolution of dislocation cores and crack fronts are critical to a more fundamental understanding of the physics of plasticity and failure. However, even the treatment of submicron cracks and dislocation loops by atomistic methods is generally not feasible today because of the large number of atoms required. While concurrent models such as those of Abraham *et al*. [1] and Khare *et al*. [2] can deal with defects of moderate size, on the order of hundreds of

*Correspondence to: Ted Belytschko, Department of Mechanical Engineering, Northwestern University, 2145 Sheridan Road, Evanston, IL 60208-3111, U.S.A.
†E-mail: tedbelytschko@northwestern.edu

Contract/grant sponsor: Army Research Office; contract/grant numbers: W911NF-05-1-0049, W911NF-08-1-0212

Angstroms, this does not suffice for many dislocation and crack problems of interest. A key need is for methods that can apply atomistic models where needed and apply continuum models to the remainder of the domain with the capability to model the discontinuities associated with cracks and dislocations.

In this paper, a method is proposed that couples discontinuous continuum models for cracks and dislocations with atomistic models. The objective is to model crack fronts and dislocation cores by atomistics, and in the rest of the domain use a continuum model. This is accomplished by adding discontinuities to the continuum model, which are coincident with the discontinuities that result from cracks or dislocations. The discontinuities can be arbitrarily oriented with respect to the discretization of the continuum. The capability of this method to model arbitrary discontinuities with ease enables the atomistic domain to be limited to the small region where bond breaking and formation takes place.

Ultimately, the objective is to extend the method so that propagating crack tips and dislocation cores can be modeled with the atomistics employed only where needed—in the spirit of model adaptivity proposed by Oden *et al.* [3]. Thus, in modeling a moving dislocation, the core would be modeled by an atomistic model and the remainder of the domain would be modeled by a continuum. As the dislocation core moves, atomistic models would be activated in certain subdomains and deactivated by reverting to a continuum model in other subdomains.

Reviews of previous work on coupled atomistic/continuum models can be found in [4–6]. In the following, we will only review methods aimed at similar problems and some of the issues involved.

One of the most popular coupled continuum/atomistic methods is the quasicontinuum method of Tadmor *et al*. [7]. This method has been applied to a variety of defect problems, including dislocations [8, 9]. The method seamlessly blends atomics with continuum finite elements (FE) by switching from a continuum potential to a force-field potential. However, the method requires the nodes in the atomistic region to coincide with the atoms, which can lead to meshing difficulties since the mesh must be severely gradated to take advantage of the smaller resolution requirements away from a defect. Since dislocations that are nucleated in the atomistic domain tend to propagate toward the continuum domain, large portions of the initial continuum domain must be converted to atomistics. This can lead to situations where the number of atomistic degrees of freedom increases prohibitively.

To circumvent this difficulty, the Continuum Atomistic Dislocation Dynamics (CADD) method has been developed [10, 11]. This method couples an atomistic model to a continuum model in the same way as the quasicontinuum method; in addition, the continuum model is augmented by the dislocation dynamics model of van der Giessen and Needleman [12]. A dislocation core is treated in the continuum by superposing the analytic solution of an edge dislocation in an infinite domain with an FE solution via traction boundary conditions. The method has many interesting features and has been used to solve some important problems, such as nanoindentation. Though the CADD method is able to drastically reduce the number of atomistic degrees of freedom, it does so at the expense of introducing a singularity at the dislocation cores in the continuum and rules are needed to model short-range interactions of dislocations in the continuum domain. It also depends on a phenomenological equation of motion to govern the motion of dislocations in the continuum. Furthermore, it seems that the CADD method cannot be easily extended to three-dimensional analysis.

The proposed method is similar to the CADD method in that slip away from the cores is modeled by the continuum displacement field and so a large number of atomistic degrees of freedom are removed from the simulation. However, in the proposed method discontinuities are directly



DOI: 10.1002/nme

introduced into the displacement field and all dislocation cores are handled by atomistics and so it does not require an analytical solution. Furthermore, anisotropic continua can be treated, the energy at dislocation cores is finite and short-range interactions and propagation can be naturally handled by the atomistic model.

The coupled atomistic/continuum method with arbitrary discontinuities is constructed by combining the bridging domain method (BDM) [13–16] with the extended finite element method (XFEM) [17, 18]. The method was first presented by the authors in [19]. A similar method for combining XFEM with atomistics for dynamic crack propagation was presented at the same time by Aubertin *et al*. [20].

The XFEM is able to model arbitrary discontinuities by introducing discontinuous functions into the approximation space through the Partition of Unity framework [21]. It allows discontinuities such as cracks [17, 18] and dislocations [22–24] to be represented independently of the discretization. XFEM is closely related to the generalized finite element method [25].

The BDM is an overlapping domain decomposition scheme where compatibility between the atomistic and continuum domains is enforced using Lagrange multipliers. It has been used to study defects and cracks in graphene and carbon nanotubes [13–16] and dislocation nucleation about a void [26]. The BDM is similar to the earlier Arlequin method [27], which couples continuum models, although the BDM uses a linear weighting of the energies in the coupling domain. The atomistic-to-continuum force-based blending method described in [26, 28] is similar to the BDM described in [15], but Badia *et al.* [28] point out for the first time that proper weighting of the energy of the atomic bonds in needed to satisfy the patch test.

Overlapping domain decomposition schemes offer some distinct advantages over interface coupling methods such as the quasicontinuum method. Methods in which the FE mesh needs to be refined to the atomistic lattice dimensions near a defect are cumbersome, especially for complicated crystals such as graphene or almost any crystal in three dimensions. In addition, overlapping domain decomposition schemes allow *hot spots* to be easily activated and deactivated during the course of an analysis.

We will consider numerical examples involving defects in graphene sheets. The model described here should be an attractive alternative to mesoscale continuum models of defected graphene [29, 30] because it models the core of the dislocation more accurately.

We end this introduction with a few words about the use of a concurrent scheme versus an hierarchical multiscale scheme. In this paper a concurrent multiscale method is described. A concurrent scheme is adopted because in general hierarchical multiscale models become inapplicable once the atomistic model loses stability, i.e. at the onset of failure. Recently, Belytschko *et al.* [31] have developed two scale methods that allow for loss of stability (failure) in the micro-scale model; however, further development of these ideas is required.

This paper is organized as follows: in the following section we introduce the governing equations; in Sections 3, 4 and 5 the field variable approximations, the discrete equations and some implementation guidelines are given, respectively. In Section 6 three problems are solved to demonstrate the accuracy and the application of the described coupling scheme; Section 7 gives our conclusions.

## 2. MODEL AND GOVERNING EQUATIONS

A typical model for this method is shown in Figure 1, which illustrates a crack with an edge dislocation emanating from the crack tip. The crack tip and dislocation cores are modeled by



DOI: 10.1002/nme

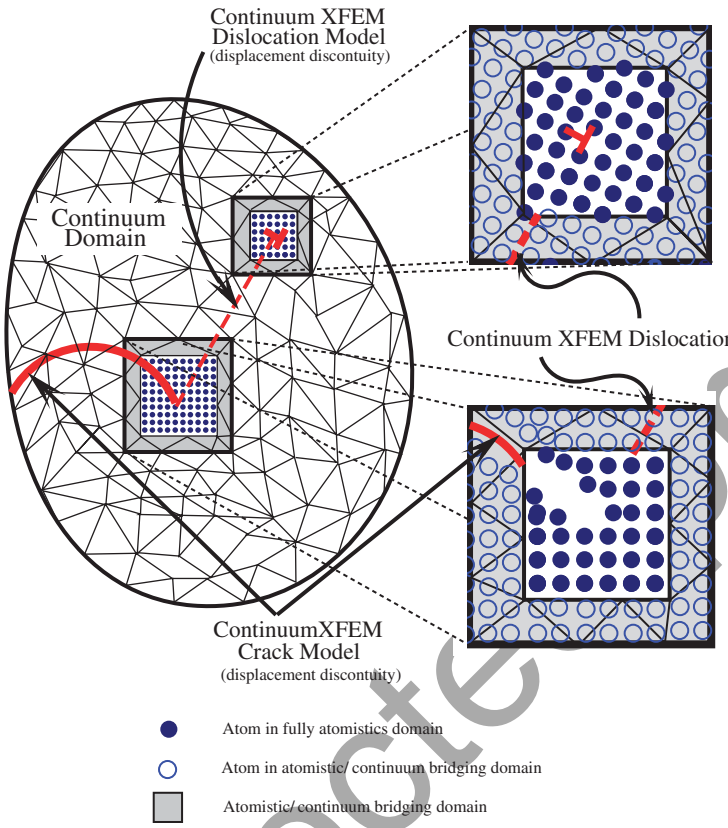


Figure 1. Schematic of a coupled extended finite element method and bridging domain method continuum/atomistic model of an edge dislocation emanating from a crack tip.



atomistics. The portion of the crack behind the crack tip and the slip between the crack tip and the dislocation core are modeled by XFEM. Around each fully atomistic subdomain is a *bridging domain* where both an atomistic and a continuum model exist. In the bridging subdomains, compatibility between the atomistic and continuum models is enforced and the energies of the atomistic and continuum models are scaled so that energy is not counted twice. Note that the crack and the glide plane are completely independent of the FE mesh; the elements are larger than the lattice spacing and the FE mesh does not conform to the lattice.

The domain of the model is denoted by $\Omega$ with boundary $\partial\Omega$, as shown in Figure 2. The domain is decomposed into overlapping subdomains $\Omega^{\mathrm{C}}$, where a continuum approximation is used, and $\Omega^{\mathrm{A}}$, where a molecular mechanics model of the material structure and behavior is used. Continuity between the atomistic and the continuum models is enforced in the bridging domain, $\Omega^{\mathrm{B}} = \Omega^{\mathrm{C}} \cap \Omega^{\mathrm{A}}$, by Lagrange multipliers. For simplicity, we will assume that the boundary $\partial\Omega^{\mathrm{A}}$ of $\Omega^{\mathrm{A}}$ does not intersect the boundary of the domain, i.e. $\partial\Omega \cap \partial\Omega^{\mathrm{A}} = 0$. On $\partial\Omega_u \subseteq \partial\Omega$ displacements $\bar{\mathbf{u}}$ are prescribed and on $\partial\Omega_t \subseteq \partial\Omega$, $\partial\Omega_t \cap \partial\Omega_u = 0$, tractions $\mathbf{t} = \bar{\mathbf{t}}$ are applied. Furthermore, the



DOI: 10.1002/nme

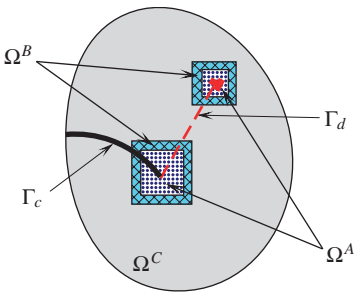


Figure 2. Schematic of a multiscale problem in which the domain contains a crack $\Gamma_c$ and a dislocation; the dislocation glide plane is denoted by $\Gamma_d$. In the regions near the crack tip and the dislocation core, denoted by $\Omega^A$, atomistic models are adopted, while in the rest of the domain, $\Omega^C$, a continuum is used. The continuum $\Omega^C$ and atomistic $\Omega^A$ domains overlap on $\Omega^B$, where compatibility between the different models is enforced.

subdomain $\Omega^C$ contains $n^d$ dislocations and $n^c$ cracks. The portion of the glide plane of dislocation $i$ where slip has occurred is denoted by $\Gamma_d^i$ and $\Gamma_d = \bigcup_{i=1}^{n^d} \Gamma_d^i$. The Burgers vector for dislocation $i$ is denoted as $\mathbf{b}^i$. The $j$th crack is denoted by $\Gamma_c^j$ and $\Gamma_c = \bigcup_{j=1}^{n^c} \Gamma_c^j$. In this paper, we have considered linear continua, since for the phenomena of interest the material in the continuum domain is well represented by linear elasticity; however, the method can easily be extended to the fully non-linear case. The material in the atomistic domain is governed by a non-linear interatomic potential and so it is fully non-linear.

Let the continuum displacement field be denoted by $\mathbf{u}(\mathbf{x}), \mathbf{x} \in \Omega^C$; we will assume small displacement behavior of the continuum and so we will not differentiate between material and reference coordinates. Let $\mathscr{S}^A$, $\mathscr{S}^B$ and $\mathscr{S}^{AB}$ be the sets of all atoms in $\Omega^A$, all atoms in $\Omega^B$ and all atoms in $\Omega^A \backslash \Omega^B$, respectively. The position vector of atom $\alpha$ is denoted by $\mathbf{x}_\alpha^A$ and its displacement is denoted by $\mathbf{u}_\alpha^A$. We group the atomistic displacements into a column matrix $\mathbf{d}^{A\top} = \{\mathbf{u}_1^A, \mathbf{u}_2^A, \ldots, \mathbf{u}_{n_A}^A\}$, where $n_A$ is the number of atoms in $\mathscr{S}^A$. The Lagrange multiplier field is denoted by $\boldsymbol{\lambda}(\mathbf{x}), \mathbf{x} \in \Omega^B$.

The energies of the continuum and atomistic models are, respectively, weighted by $w^C(\mathbf{x})$ and $w^A(\mathbf{x})$, which must satisfy the conditions:

$$w^A(\mathbf{x}) + w^C(\mathbf{x}) = 1 \quad \forall \mathbf{x} \in \Omega \tag{1a}$$

$$0 \leqslant w^C(\mathbf{x}) \leqslant 1 \quad \forall \mathbf{x} \in \Omega \tag{1b}$$

$$0 \leqslant w^A(\mathbf{x}) \leqslant 1 \quad \forall \mathbf{x} \in \Omega \tag{1c}$$

$$w^C(\mathbf{x}) = 1 \quad \forall \mathbf{x} \in \Omega^C \backslash \Omega^B \tag{1d}$$

$$w^A(\mathbf{x}) = 1 \quad \forall \mathbf{x} \in \Omega^A \backslash \Omega^B \tag{1e}$$

Conditions (1a)–(1c) ensure that the energy at a point $\mathbf{x}$ is only counted once, while conditions (1d)–(1e) ensure that only the continuum approximation contributes to the total energy in the subdomain $\Omega^C \backslash \Omega^B$ and that only the atomistic approximation contributes to the total energy in the





DOI: 10.1002/nme

subdomain $\Omega^A \backslash \Omega^B$. The weight functions $w^C(\mathbf{x})$ and $w^A(\mathbf{x})$ vary monotonically between 0 and 1 in the bridging domain $\Omega^B$. The specific form of $w^C(\mathbf{x})$ and $w^A(\mathbf{x})$ will be given later.

Using the definitions of the weight functions (1), we can also define the continuum, atomistic and bridging domains as:

$$\Omega^C = \{\mathbf{x} \in \Omega | 0 < w^C(\mathbf{x}) \leqslant 1\} \tag{2a}$$

$$\Omega^A = \{\mathbf{x} \in \Omega | 0 < w^A(\mathbf{x}) \leqslant 1\} \tag{2b}$$

$$\Omega^B = \{\mathbf{x} \in \Omega | 0 < w^A(\mathbf{x}) < 1\} \tag{2c}$$

Definitions (2) allow *hot spots* to be activated and deactivated by modifying the definitions of $w^C(\mathbf{x})$ and $w^A(\mathbf{x})$ during the course of a simulation.

The total energy of the system is given by

$$\Pi(\mathbf{u}, \mathbf{d}^A, \boldsymbol{\lambda}) = \Pi^C(\mathbf{u}) + \Pi^A(\mathbf{d}^A) + \Pi^B(\mathbf{u}, \mathbf{d}^A, \boldsymbol{\lambda}) \tag{3}$$

where $\Pi^C$ is the energy from the continuum model in $\Omega^C$, $\Pi^A$ is the potential energy from the atomistic model in $\Omega^A$ and $\Pi^B$ is the Lagrange multiplier constraint that enforces compatibility between the atomistic and continuum models in $\Omega^B$. Equation (3) is subject to the boundary and interior conditions

$$\mathbf{u}(\mathbf{x}) = \bar{\mathbf{u}} \quad \forall \mathbf{x} \in \partial\Omega_u \tag{4a}$$

$$\boldsymbol{\sigma}(\mathbf{x}) \cdot \mathbf{n} = \bar{\mathbf{t}} \quad \forall \mathbf{x} \in \partial\Omega_t \tag{4b}$$

$$\boldsymbol{\sigma}(\mathbf{x}) \cdot \mathbf{n} = 0 \quad \forall \mathbf{x} \in \Gamma_c \tag{4c}$$

$$[|\mathbf{u}(\mathbf{x})|] = \mathbf{b} \quad \forall \mathbf{x} \in \Gamma_d \tag{4d}$$

where $\boldsymbol{\sigma}$ is the Cauchy stress, $\mathbf{n}$ is the outward facing normal to $\partial\Omega_t$ and $[|\mathbf{u}(\mathbf{x})|]$ represents the jump in the displacements. Condition (4c) imposes traction-free boundary conditions on all crack faces in the continuum; this condition can be replaced by a cohesive crack model. Here, for simplicity we assume that all cohesive behavior occurs in $\Omega^A \backslash \Omega^B$ and so no cohesive force conditions are necessary. Condition (4d) ensures that the slip along the glide plane in the continuum is equal to the Burgers vector.

The energy of the continuum model is given by

$$\Pi^C(\mathbf{u}) = \int_{\Omega^C} w^C(\mathbf{x}) W^C(\mathbf{u}(\mathbf{x})) \, \mathrm{d}\Omega - W^{\mathrm{ext}} \tag{5}$$

where $W^C(\mathbf{x})$ is the strain energy density and $W^{\mathrm{ext}}$ is the work of external loads. The linearized strain is denoted by $\boldsymbol{\varepsilon}$ and is defined as $\varepsilon_{ij} = \frac{1}{2}(u_{i,j} + u_{j,i})$, where a comma denotes differentiation. The stain energy density is given by

$$W^C(\mathbf{x}) = \tfrac{1}{2} \varepsilon_{ij}(\mathbf{x}) \sigma_{ij}(\mathbf{x}) \tag{6}$$

In this paper we will assume a linear elastic constitutive law; however, the framework can easily consider a non-linear hyperelastic continuum where the stress is determined by the Cauchy–Born



DOI: 10.1002/nme

rule [7, 32]. Similarly, the effects of free surfaces can be incorporated through a surface Cauchy–Born rule [33] and the cohesive tractions across continuum crack surfaces can be modeled by a cohesive Cauchy–Born rule [34].

The contribution to the total energy from the atomistic model is

$$\Pi^{\mathrm{A}}(\mathbf{d}^{\mathrm{A}}) = \frac{1}{2}\sum_{\alpha=1}^{n_{\mathrm{A}}}\sum_{\beta\neq\alpha}^{n_{\mathrm{A}}+n_{\mathrm{G}}} w_{\alpha\beta}^{\mathrm{A}} V(\mathbf{x}_{\alpha}^{\mathrm{A}}, \mathbf{x}_{\beta}^{\mathrm{A}}) \tag{7}$$

where $n_{\mathrm{G}}$ is the number of *ghost* or *pad* atoms, $V$ is the functional governing two-body interactions (this assumption is not necessary, but simplifies the remaining development) and $w_{\alpha\beta}^{\mathrm{A}}$ is defined as

$$w_{\alpha\beta}^{\mathrm{A}} = \tfrac{1}{2}(w^{\mathrm{A}}(\mathbf{x}_{\alpha}^{\mathrm{A}}) + w^{\mathrm{A}}(\mathbf{x}_{\beta}^{\mathrm{A}})) \tag{8}$$

An atom $\gamma$ is a ghost atom if $w^{\mathrm{A}}(\mathbf{x}_{\gamma}^{\mathrm{A}}) = 0$ and there exists an atom $\beta$ such that $w_{\gamma\beta}^{\mathrm{A}} \neq 0$ and $V(\mathbf{x}_{\alpha}^{\mathrm{A}}, \mathbf{x}_{\beta}^{\mathrm{A}}) \neq 0$; i.e. ghost atoms reside in the fully continuum domain $\Omega^{\mathrm{C}}\backslash\Omega^{\mathrm{B}}$, but are sufficiently close to the atomistic domain $\Omega^{\mathrm{A}}$ that they interact with atoms in $\Omega^{\mathrm{A}}$. The positions of the ghost atoms are not free degrees of freedom; their positions are interpolated using the continuum displacement field (10).

The coupling constraint is given by

$$\Pi^{\mathrm{B}}(\mathbf{u}, \mathbf{d}^{\mathrm{A}}, \boldsymbol{\lambda}) = \sum_{\alpha\in\mathscr{S}^{\mathrm{B}}} \int_{\Omega^{\mathrm{B}}} \boldsymbol{\lambda}(\mathbf{x}) \cdot [\mathbf{u}(\mathbf{x}) - \mathbf{u}_{\alpha}^{\mathrm{A}}] \delta(\mathbf{x} - \mathbf{x}_{\alpha}^{\mathrm{A}})\, \mathrm{d}\Omega \tag{9a}$$

$$= \sum_{\alpha\in\mathscr{S}^{\mathrm{B}}} \boldsymbol{\lambda}(\mathbf{x}_{\alpha}^{\mathrm{A}}) \cdot [\mathbf{u}(\mathbf{x}_{\alpha}^{\mathrm{A}}) - \mathbf{u}_{\alpha}^{\mathrm{A}}] \tag{9b}$$

## 3. DISCRETE APPROXIMATIONS

In this section we describe the discretization for a domain containing a single dislocation and a single crack, as shown in Figure 2, to facilitate the presentation of the equations. The generalization to many cracks or dislocations is straight forward. Let the zero contour of the function $\phi(\mathbf{x})$ define the location of the crack, i.e. $\Gamma_{\mathrm{c}} = \{\mathbf{x} \in \Omega^{\mathrm{C}} | \phi(\mathbf{x}) = 0\}$. Similarly, let the zero contour of the function $\psi(\mathbf{x})$ define the location of the portion of the dislocation glide plane where slip has occurred, i.e. $\Gamma_{\mathrm{d}} = \{\mathbf{x} \in \Omega^{\mathrm{C}} | \psi(\mathbf{x}) = 0\}$. We assume that cracks and dislocations begin and end either at the domain boundary or in the fully atomistic domain $\Omega^{\mathrm{A}}\backslash\Omega^{\mathrm{B}}$.

### *3.1. Continuum displacement approximation*

The subdomain $\Omega^{\mathrm{C}}$ is discretized by the set of elements $\mathscr{E}$ with nodes $\mathscr{N}$. Let $\mathbf{x}_I$ be the position of node $I$. The continuum displacement approximation is additively decomposed into continuous and discontinuous parts; therefore,

$$\mathbf{u}(\mathbf{x}) = \mathbf{u}^{\mathrm{C}}(\mathbf{x}) + \mathbf{u}^{\mathrm{D}}(\mathbf{x}) \quad \forall \mathbf{x} \in \Omega^{\mathrm{C}} \tag{10}$$

The continuous part, $\mathbf{u}^{\mathrm{C}}(\mathbf{x})$, is given by the standard FE approximation

$$\mathbf{u}^{\mathrm{C}}(\mathbf{x}) = \sum_{I\in\mathscr{N}} N_I(\mathbf{x})\mathbf{u}_I \quad \forall \mathbf{x} \in \Omega^{\mathrm{C}} \tag{11}$$



DOI: 10.1002/nme

where $N_I$ are the nodal shape functions and $\mathbf{u}_I$ are the standard nodal degrees of freedom. Approximations of the form (10) were first considered by Fish [35] for cracks and also constitute an important element of the XFEM [18].

The discontinuous part of the displacement approximation is further decomposed into two parts

$$\mathbf{u}^{\mathrm{D}}(\mathbf{x}) = \mathbf{u}^{\mathrm{Dd}}(\mathbf{x}) + \mathbf{u}^{\mathrm{Dc}}(\mathbf{x}) \quad \forall \mathbf{x} \in \Omega^{\mathrm{C}} \tag{12}$$

where $\mathbf{u}^{\mathrm{Dd}}$ is the enrichment for the dislocation in the continuum

$$\mathbf{u}^{\mathrm{D1}}(\mathbf{x}) = \mathbf{b} \sum_{J \in \mathcal{N}^{\psi}} N_J(\mathbf{x})[H(\psi(\mathbf{x})) - H_J^{\psi}] \quad \forall \mathbf{x} \in \Omega^{\mathrm{C}} \tag{13}$$

and $\mathbf{u}^{\mathrm{Dc}}$ is the enrichment for the crack in the continuum

$$\mathbf{u}^{\mathrm{D2}}(\mathbf{x}) = \sum_{K \in \mathcal{N}^{\phi}} N_K(\mathbf{x})[H(\phi(\mathbf{x})) - H_K^{\phi}]\mathbf{a}_K \quad \forall \mathbf{x} \in \Omega^{\mathrm{C}} \tag{14}$$

where $\mathcal{N}^{\psi} \subseteq \mathcal{N}$ and $\mathcal{N}^{\phi} \subseteq \mathcal{N}$ are the sets of nodes with supports cut by $\Gamma_{\mathrm{d}}$ and $\Gamma_{\mathrm{c}}$, respectively. $H(\cdot)$ is the Heaviside step function, $H_J^{\psi} = H(\psi(\mathbf{x}_J))$ and $H_J^{\phi} = H(\phi(\mathbf{x}_J))$. Equation (13) introduces a displacement discontinuity with magnitude and direction of the Burgers vector across the glide plane. This part of the approximation is the XFEM dislocation model introduced in [23]. Equation (14) introduces a displacement discontinuity along the crack using the XFEM approximation as introduced in [18]. The additional nodal degrees of freedom $\mathbf{a}_K$ are related to the magnitude of the crack opening displacement. The shifting of the enrichment, seen in the square brackets in Equations (13) and (14), is done so that (13) and (14) are only non-zero in those elements that are cut by either $\Gamma_{\mathrm{d}}$ or $\Gamma_{\mathrm{c}}$, respectively. Shifting has the additional benefit of making $\mathbf{u}(\mathbf{x}_J) = \mathbf{u}_J$ and so essential boundary conditions can be approximated by constraining the standard nodal degrees of freedom $\mathbf{u}_J$. A key feature of the XFEM approximation is that the discontinuities due to cracks and dislocations are independent of the FE mesh.

### *3.2. Lagrange multiplier approximation*

Compatibility, in the blending domain $\Omega^{\mathrm{B}}$, between the discrete atomistic displacements and that of the continuum can be enforced exactly by associating one Lagrange multiplier with each degree of freedom of each atom in $\Omega^{\mathrm{B}}$. This constraint may be too strict [36, 37]. In this paper, we enforce compatibility weakly by approximating the Lagrange multipliers by fields similar to [13]. Based on work conjugacy, the Lagrange multipliers can be physically identified as forces that act to reduce the incompatibility between the atomistic and continuum displacements. To approximate the Lagrange multiplier field, we discretized $\Omega^{\mathrm{B}}$ by a set of elements $\mathscr{E}^{\lambda}$ with nodes $\mathscr{M}$.

When the strains in the bridging subdomain $\Omega^{\mathrm{B}}$ are continuous, the Lagrange multipliers can be approximated by a continuously varying force field. This is true even when $\Gamma_{\mathrm{d}}$ passes through $\Omega^{\mathrm{B}}$ (as long as no dislocation cores are in $\Omega^{\mathrm{B}}$). One can explain this by recalling that the strain and stress fields due to dislocations are continuous everywhere except at the dislocation cores. When a crack $\Gamma_{\mathrm{c}}$ passes through $\Omega^{\mathrm{B}}$ both the displacements and strains on either side of the crack will evolve independently and so one may be tempted to use a Lagrange multiplier field approximation that is discontinuous (similar to the XFEM crack approximation). However, a discontinuous Lagrange multiplier approximation actually decreases the accuracy for the examples considered here because a discontinuous approximation more stringently enforces compatibility between the continuum and





DOI: 10.1002/nme

the atomistic model. Often this would be preferable, but the atomistic model relaxes along the crack surfaces, whereas the continuum model does not; therefore, stringently enforcing compatibility results in the continuum model resisting the relaxation of the atomistic model, thereby increasing the energy stored in the system.

Therefore, we use a continuous approximation for the Lagrange multiplier field of the form

$$\boldsymbol{\lambda}(\mathbf{x}) = \sum_{I \in \mathscr{M}} N_I^{\lambda}(\mathbf{x}) \boldsymbol{\lambda}_I \quad \forall \mathbf{x} \in \Omega^{\mathrm{B}} \tag{15}$$

where $N_I^{\lambda}$ are the Lagrange multiplier nodal shape functions and $\boldsymbol{\lambda}_I$ are the Lagrange multiplier nodal degrees of freedom.

### *3.3. Energy weight functions*

The energy weighting functions $w^{\mathrm{C}}(\mathbf{x})$ and $w^{\mathrm{A}}(\mathbf{x})$ are defined with FE shape functions. We consider a discretization of the total domain $\Omega$ by a set of elements $\mathscr{E}^{\Omega}$ with nodes $\mathscr{N}^{\Omega}$:

$$w^{\mathrm{C}}(\mathbf{x}) = \sum_{I \in \mathscr{N}^{\Omega}} N_I(\mathbf{x}) w_I^{\mathrm{C}} \quad \forall \mathbf{x} \in \Omega \tag{16}$$

where $w^{\mathrm{A}}(\mathbf{x})$ is defined by (16) and (1)—$w^{\mathrm{A}}(\mathbf{x}) = 1 - w^{\mathrm{C}}(\mathbf{x})$. Furthermore, we define $\mathscr{N} \subseteq \mathscr{N}^{\Omega}$ and $\mathscr{E} \subseteq \mathscr{E}^{\Omega}$. The fully atomistic domain is then defined by the set of elements $e$ where $w_I^{\mathrm{C}} = 0$ for each node of element $e$. The definition of $w^{\mathrm{C}}(\mathbf{x})$ by (16) implies that $w^{\mathrm{C}}(\mathbf{x})$ and $w^{\mathrm{A}}(\mathbf{x})$ are piecewise linear since we will adopt linear shape functions $N_I$. The elements $\mathscr{E}^{\lambda}$ and nodes $\mathscr{M}$ of the Lagrange multiplier mesh are chosen to coincide with the displacement field elements $\mathscr{E}$ where $0 < w^{\mathrm{C}}(\mathbf{x}) < 1$. In the examples presented here, the bridging domain is one element wide; therefore, $w_I^{\mathrm{C}}$ is defined by (1) and (16). For wider blending domains, orthogonal projection techniques such as those given in [38] can be used.

## 4. DISCRETE EQUATIONS

The solution is obtained by finding the stationary point of the total energy functional (3) given the field approximations (10)–(12), (15) and the boundary conditions (4). Since (3) is a Lagrange multiplier problem, the solution is a saddle point, and so cannot be obtained using conjugate gradient-based solvers. To circumvent this difficulty, we adopt the staggered solution scheme described in [16]. Alternatively, Equation (3) may be recast in an augmented Lagrangian form as in [14].

We begin by defining two subproblems, which we associate with two energy functionals $\Pi^1$ and $\Pi^2$. $\Pi^1$ and $\Pi^2$ are the same energy functionals as (3) except that in the case of $\Pi^1$ all atomistic degrees of freedom are fixed and in the case of $\Pi^2$ all continuum degrees of freedom and all Lagrange multiplier degrees of freedom are fixed, i.e.

$$\Pi^1(\mathbf{u}, \boldsymbol{\lambda}) = \Pi(\mathbf{u}, \mathbf{d}^{\mathrm{A}}, \boldsymbol{\lambda}) \tag{17a}$$

$$\Pi^2(\mathbf{d}^{\mathrm{A}}) = \Pi(\mathbf{u}, \mathbf{d}^{\mathrm{A}}, \boldsymbol{\lambda}) \tag{17b}$$



DOI: 10.1002/nme

### 4.1. Subproblem 1

The governing equations for $\Pi^1(\mathbf{u}, \boldsymbol{\lambda})$ are obtained by substituting (10)–(12) and (15) into (17a) and setting the derivatives of $\Pi^1(\mathbf{u}, \boldsymbol{\lambda})$ with respect to $\mathbf{u}_I$, $\mathbf{a}_I$ and $\boldsymbol{\lambda}_L$ equal to zero:

$$\frac{\partial \Pi^1(\mathbf{d}^{\mathrm{C}}, \mathbf{d}^{\mathrm{D}}, \mathbf{q})}{\partial \mathbf{u}_I} = 0 \quad \forall I \in \mathcal{N} \tag{18a}$$

$$\frac{\partial \Pi^1(\mathbf{d}^{\mathrm{C}}, \mathbf{d}^{\mathrm{D}}, \mathbf{q})}{\partial \mathbf{a}_I} = 0 \quad \forall I \in \mathcal{N}^{\phi} \tag{18b}$$

$$\frac{\partial \Pi^1(\mathbf{d}^{\mathrm{C}}, \mathbf{d}^{\mathrm{D}}, \mathbf{q})}{\partial \boldsymbol{\lambda}_L} = 0 \quad \forall L \in \mathcal{M} \tag{18c}$$

where

$$\mathbf{d}^{\mathrm{C}\top} = \{\mathbf{u}_1^{\mathrm{C}}, \mathbf{u}_2^{\mathrm{C}}, \ldots, \mathbf{u}_n^{\mathrm{C}}\} \tag{19a}$$

$$\mathbf{d}^{\mathrm{D}\top} = \{\mathbf{a}_1, \mathbf{a}_2, \ldots, \mathbf{a}_{n2}\} \tag{19b}$$

$$\mathbf{q}^{\top} = \{\boldsymbol{\lambda}_1, \boldsymbol{\lambda}_2, \ldots, \boldsymbol{\lambda}_m\} \tag{19c}$$

and $n$, $n2$ and $m$ are the number of nodes in the sets $\mathcal{N}$, $\mathcal{N}^{\phi}$ and $\mathcal{M}$, respectively. We note that no equations in (18) are associated with the partial derivative of $\Pi^1(\mathbf{u}, \boldsymbol{\lambda})$ with respect to the Burgers vector $\mathbf{b}$, which appears in (12). In continuum dislocation models, $\mathbf{b}$ is obtained from the lattice slip due to the dislocation.

Problem 1 yields a linear system of equations; in matrix form these equations are

$$\begin{bmatrix} \mathbf{K}^{\mathrm{CC}} & \mathbf{K}^{\mathrm{CD}} & \mathbf{G}^{\mathrm{C}} \\ \mathbf{K}^{\mathrm{CD}\top} & \mathbf{K}^{\mathrm{DD}} & \mathbf{G}^{\mathrm{D}} \\ \mathbf{G}^{\mathrm{C}\top} & \mathbf{G}^{\mathrm{D}\top} & \mathbf{0} \end{bmatrix} \begin{Bmatrix} \mathbf{d}^{\mathrm{C}} \\ \mathbf{d}^{\mathrm{D}} \\ \mathbf{q} \end{Bmatrix} + \begin{Bmatrix} \mathbf{0} \\ \mathbf{0} \\ \mathbf{f}^{\lambda} \end{Bmatrix} + \begin{Bmatrix} \mathbf{f}^{\mathrm{C,d}} \\ \mathbf{f}^{\mathrm{D,d}} \\ \mathbf{g}^{\mathrm{d}} \end{Bmatrix} = \begin{Bmatrix} \mathbf{f}^{\mathrm{C,ext}} \\ \mathbf{f}^{\mathrm{D,ext}} \\ \mathbf{0} \end{Bmatrix} \tag{20}$$

The stiffness matrices are given by

$$\mathbf{K}_{IJ}^{\mathrm{CC}} = \int_{\Omega^{\mathrm{C}}} w^{\mathrm{C}} \mathbf{B}_I^{\top} \mathbf{C} \mathbf{B}_J \, \mathrm{d}\Omega, \quad I, J \in \mathcal{N} \tag{21}$$

$$\mathbf{K}_{IJ}^{\mathrm{CD}} = \int_{\Omega^{\mathrm{C}}} w^{\mathrm{C}} \mathbf{B}_I^{\top} \mathbf{C} \widetilde{\mathbf{B}}_J \, \mathrm{d}\Omega, \quad I \in \mathcal{N}, \quad J \in \mathcal{N}^{\phi} \tag{22}$$

$$\mathbf{K}_{IJ}^{\mathrm{DD}} = \int_{\Omega^{\mathrm{C}}} w^{\mathrm{C}} \widetilde{\mathbf{B}}_I^{\top} \mathbf{C} \widetilde{\mathbf{B}}_J \, \mathrm{d}\Omega, \quad I, J \in \mathcal{N}^{\phi} \tag{23}$$





DOI: 10.1002/nme

where $\mathbf{C}$ is the Hookean matrix and in two dimensions

$$\mathbf{B}_I = \begin{bmatrix} N_{I,x} & 0 \\ 0 & N_{I,y} \\ N_{I,y} & N_{I,x} \end{bmatrix} \tag{24}$$

$$\widetilde{\mathbf{B}}_I = \begin{bmatrix} (N_I[H(\phi(\mathbf{x}))-H_I^{\phi}])_{,x} & 0 \\ 0 & (N_I[H(\phi(\mathbf{x}))-H_I^{\phi}])_{,y} \\ (N_I[H(\phi(\mathbf{x}))-H_I^{\phi}])_{,y} & (N_I[H(\phi(\mathbf{x}))-H_I^{\phi}])_{,x} \end{bmatrix} \tag{25}$$

and a comma denotes differentiation.

The continuum–atomistic coupling stiffness matrices are

$$\mathbf{G}_{IL}^{\mathrm{C}} = \sum_{\alpha\in\mathscr{S}^{\mathrm{B}}} N_L^{\lambda}(\mathbf{x}_\alpha^{\mathrm{A}}) N_I(\mathbf{x}_\alpha^{\mathrm{A}}), \quad I\in\mathscr{N}, \;\; L\in\mathscr{M} \tag{26}$$

$$\mathbf{G}_{IL}^{\mathrm{D}} = \sum_{\alpha\in\mathscr{S}^{\mathrm{B}}} N_L^{\lambda}(\mathbf{x}_\alpha^{\mathrm{A}}) N_I(\mathbf{x}_\alpha^{\mathrm{A}})[H(\phi(\mathbf{x}_\alpha^{\mathrm{A}}))-H_I^{\phi}], \quad I\in\mathscr{N}^{\phi}, \;\; L\in\mathscr{M} \tag{27}$$

The external nodal forces are

$$\mathbf{f}^{\mathrm{C,ext}} = \int_{\partial\Omega_t} w^{\mathrm{C}} \mathbf{N}_I^{\top} \bar{\mathbf{t}}\, \mathrm{d}\Omega, \quad I\in\mathscr{N} \tag{28}$$

$$\mathbf{f}^{\mathrm{D,ext}} = \int_{\partial\Omega_t} w^{\mathrm{C}} \mathbf{N}_I^{\top} [H(\phi(\mathbf{x}))-H_I^{\phi}] \bar{\mathbf{t}}\, \mathrm{d}\Omega, \quad I\in\mathscr{N}^{\phi} \tag{29}$$

and the nodal forces due to the atoms acting on the continuum through the Lagrange multipliers are

$$\mathbf{f}_L^{\lambda} = -\sum_{\alpha\in\mathscr{S}^{\mathrm{B}}} N_L^{\lambda}(\mathbf{x}_\alpha^{\mathrm{A}}) \mathbf{u}_\alpha^{\mathrm{A}}, \quad L\in\mathscr{M} \tag{30}$$

The nodal forces due to the dislocations in the continuum are

$$\mathbf{f}_I^{\mathrm{C,d}} = \int_{\Omega^{\mathrm{C}}} w^{\mathrm{C}} \mathbf{B}_I^{\top} \boldsymbol{\sigma}(\mathbf{u}^{\mathrm{Dd}})\, \mathrm{d}\Omega, \quad I\in\mathscr{N} \tag{31}$$

$$\mathbf{f}_I^{\mathrm{D,d}} = \int_{\Omega^{\mathrm{C}}} w^{\mathrm{C}} \widetilde{\mathbf{B}}_I^{\top} \boldsymbol{\sigma}(\mathbf{u}^{\mathrm{Dd}})\, \mathrm{d}\Omega, \quad I\in\mathscr{N}^{\phi} \tag{32}$$

where $\boldsymbol{\sigma}(\mathbf{u}^{\mathrm{Dd}})$ is the stress in the continuum due to the dislocation enrichment $\mathbf{u}^{\mathrm{Dd}}$, Equation (13). The nodal forces on the Lagrange multiplier nodes due to the continuum dislocations in the bridging domain are

$$\mathbf{g}_L^{\mathrm{d}} = \sum_{\alpha\in\mathscr{S}^{\mathrm{B}}} N_L^{\lambda}(\mathbf{x}_\alpha^{\mathrm{A}}) \mathbf{u}^{\mathrm{Dd}}(\mathbf{x}_\alpha^{\mathrm{A}}), \quad L\in\mathscr{M} \tag{33}$$





DOI: 10.1002/nme

The Lagrange multipliers in (20) are obtained by static condensation. Let

$$\mathbf{K}=\begin{bmatrix}\mathbf{K}^{\mathrm{CC}} & \mathbf{K}^{\mathrm{CD}}\\ \mathbf{K}^{\mathrm{CD}\top} & \mathbf{K}^{\mathrm{DD}}\end{bmatrix},\quad \mathbf{G}=\begin{bmatrix}\mathbf{G}^{\mathrm{C}}\\ \mathbf{G}^{\mathrm{D}}\end{bmatrix},\quad \mathbf{f}^{\mathrm{d}}=\begin{Bmatrix}\mathbf{f}^{\mathrm{C,d}}\\ \mathbf{f}^{\mathrm{D,d}}\end{Bmatrix},\quad \mathbf{f}^{\mathrm{ext}}=\begin{Bmatrix}\mathbf{f}^{\mathrm{C,ext}}\\ \mathbf{f}^{\mathrm{D,ext}}\end{Bmatrix} \tag{34}$$

The nodal Lagrange multipliers $\mathbf{q}$ are determined by

$$\mathbf{A}\mathbf{q}=\mathbf{f}^{q} \tag{35}$$

where

$$\mathbf{A}=\mathbf{G}^{\top}\mathbf{K}^{-1}\mathbf{G} \tag{36}$$

and

$$\mathbf{f}^{q}=\mathbf{f}^{\lambda}+\mathbf{g}^{\mathrm{d}}+\mathbf{G}\mathbf{K}^{-1}(\mathbf{f}^{\mathrm{ext}}-\mathbf{f}^{\mathrm{d}}) \tag{37}$$

The FEM nodal degrees of freedom, $\mathbf{d}^{\top}=\{\mathbf{d}^{\mathrm{C}},\mathbf{d}^{\mathrm{D}}\}$, are determined by substituting the solution of $\mathbf{q}$ obtained by solving the linear system (35) into (20), which gives

$$\mathbf{d}=\mathbf{K}^{-1}(\mathbf{f}^{\mathrm{ext}}-\mathbf{f}^{\mathrm{d}}-\mathbf{G}\mathbf{q}) \tag{38}$$

We use the same discretization for the Lagrange multiplier approximation, (15), as for the displacement approximation, (10)–(12), i.e. $N_I^{\lambda}(\mathbf{x})\equiv N_I(\mathbf{x})\ \ \forall\mathbf{x}\in\Omega^{\mathrm{B}}$. Following the analysis in Zhang *et al*. [16], $\mathbf{A}$ is invertible if the number of atoms in an unenriched element is greater than or equal to the number of nodes and if the number of atoms in an enriched element (i.e. one cut by a crack or a dislocation) is greater than or equal to twice the number of nodes.

### *4.2. Subproblem 2*

The equilibrium equations of $\Pi^2(\mathbf{d}^{\mathrm{A}})$ are derived by substituting approximations (10)–(12) and (15) into (17) and setting the derivatives of $\Pi^2\left(\mathbf{d}^{\mathrm{A}}\right)$ with respect to $\mathbf{x}_{\alpha}^{\mathrm{A}}$ to zero:

$$\frac{\partial\Pi^2(\mathbf{d}^{\mathrm{A}})}{\partial\mathbf{x}_{\alpha}^{\mathrm{A}}}=\bar{\mathbf{f}}_{\alpha}^{\mathrm{A}}=\mathbf{g}_{\alpha}^{\mathrm{A}}-\boldsymbol{\lambda}(\mathbf{x}_{\alpha}^{\mathrm{A}})=\mathbf{0},\quad \alpha\in\mathscr{S}^{\mathrm{A}} \tag{39}$$

where the atomistic forces acting on atoms $\alpha$ are

$$\mathbf{g}_{\alpha}^{\mathrm{A}}=\sum_{\beta=1,\beta\neq\alpha}^{n_{\mathrm{A}}+n_{\mathrm{G}}} w_{\alpha\beta}^{\mathrm{A}}\frac{\partial V}{\partial\mathbf{x}_{\alpha}^{\mathrm{A}}}(\mathbf{x}_{\alpha}^{\mathrm{A}},\mathbf{x}_{\beta}^{\mathrm{A}}),\quad \alpha\in\mathscr{S}^{\mathrm{A}} \tag{40}$$

The iterative solution of subproblems 1 and 2 follows the procedure described in [16]; it is accomplished using Algorithm 1 with the BFGS solver [39].



DOI: 10.1002/nme

*Algorithm 1* (*Discontinuous BDM*)

**foreach** *Load Step n* **do**
  i = 1
  **while** *NOT CONVERGED* **do**
    compute $\mathbf{q}_n^{(i)}$ from (35) given $\mathbf{d}_n^{\mathrm{A}(i-1)}$
    compute $\mathbf{d}_n^{(i)}$ from (38) given $\mathbf{d}_n^{\mathrm{A}(i-1)}$ and $\mathbf{q}_n^{(i)}$
    compute $\mathbf{f}_n^{\mathrm{A}(i)}$ from (39) given $\mathbf{q}_n^{(i)}$
    compute $\Pi_n^{2(i)}$ from (17b) given $\mathbf{d}_n^{(i)}$, $\mathbf{q}_n^{(i)}$ and $\mathbf{d}_n^{\mathrm{A}(i-1)}$
    compute $\mathbf{d}_n^{\mathrm{A}(i)}$ by taking one BFGS step given $\Pi_n^{2(i)}$, $\mathbf{f}_n^{\mathrm{A}(i)}$ and $\mathbf{d}_n^{\mathrm{A}(i-1)}$
    i = i+1
  **end**
**end**

## 5. IMPLEMENTATION ISSUES

There are four critical components in an implementation of the BDM:

1. The *size of the coupling domain* impacts the accuracy and the computational cost. It is desirable to limit the domain where atomistic models are used—larger bridging domains require more atomistic degrees of freedom.
2. The *discretization of the Lagrange multiplier field* is also known to significantly affect the results of the BDM. Two schemes are commonly studied: either the Lagrange multiplier field is discretized by the same mesh as the continuum displacement field or the Lagrange multiplier discretization is refined to the atomistic spacing.
3. The *constraint condition* dictates how compatibility between the continuum and the atomistic models is enforced. In the Arlequin method, an $H^1$ coupling (which involves derivatives of the Lagrange multiplier field) is generally used, while in the BDM we have found that the $L^2$ coupling is advantageous [36, 40] and so it is used here.
4. The *weight function* blends the energy from the continuum with that of the atomistics so that the energy in the coupling domain is not counted twice. Piecewise constant, linear and cubic weight functions have been adopted in the BDM.

With regard to items 1 and 2, in [37, 41] it is shown that for quasi-static problems the Lagrange multiplier discretization should at least correspond to the size of the representative volume element (RVE) of the atomistic model or the atomistic model becomes overconstrained in the bridging domain; therefore, the coupling domain should also be at least equal to the size of the RVE. Numerical studies in [41] show that increasing the size of the coupling zone only has a modest effect on the accuracy of a quantity of interest inside the atomistic domain. Therefore, one can safely reduce the size of the atomistic domain (and the number of atomistic degrees of freedom) by using a small coupling domain, about the size of an RVE. In practice, slightly larger coupling zones are more convenient when superimposing an atomistic model on an existing FE mesh.

The last two items are intricately linked. Several mathematical and numerical studies of the performance of the Arlequin and bridging domain methods have been published [27, 28, 36, 37, 40, 41]. One issue addressed by these studies is the stability of the mixed method. In [37], the continuous problems with $H^1$ coupling and $H^1$ semi-norm coupling were shown to



DOI: 10.1002/nme

satisfy the inf–sup condition; they were not able to demonstrate the inf–sup condition for the continuous problem with $L^2$ coupling. However, in [37] it is shown that the inf–sup condition is satisfied for the discrete problem with $L^2$ coupling, though the inf–sup constants are mesh dependent and tend to zero as the continuum mesh size tends to zero. This is manifested by the erratic behavior of the Lagrange multipliers field once the FE size is less than the particle spacing (see Section 5.5 of [37]). In practice this does not restrict the use of $L^2$ coupling, since elements smaller than the atomistic spacing are not useful. In addition, the displacement field solutions to numerical examples in [37] are identical for $H^1$ and $L^2$ coupling with linear and cubic weight functions. It is shown in [36] that the Arlequin method with $L^2$ coupling with a piecewise continuous weight function is unstable; however, $L^2$ coupling with a piecewise linear weight function such as that used here has been found by numerical studies to be stable. This conclusion is also applicable to the BDM [40, 41].

## 6. EXAMPLES

In this section we consider three problems that demonstrate the accuracy and usefulness of the described framework. For simplicity, our first problem involves a crack but no dislocations, while our last two problems involve only dislocations and no cracks. The study of problems involving both dislocations and cracks and evolving dislocations and cracks will be the topic of future papers.

We will study two-dimensional problems involving graphene. Multiscale simulations of graphene sheets are well suited to demonstrate the usefulness of the overlapping domain decomposition scheme since the generation of meshes that conform to the lattice is difficult. Furthermore, the simulation of defected graphene with the coupled BDM and XFEM framework will demonstrate its robustness for complex lattice structures.

We will compare the accuracy of the coupled bridging domain method and extended finite element method (XFEM-BDM) with fully atomistic direct numerical simulations (DNS). For this purpose, the change in the energy of the atoms in the fully atomistic domain due to applied loads relative to pristine unloaded sheets is considered. Let the relative error in the change in the energy per atom be defined as

$$e_\alpha^U = \frac{(U_\alpha^{\mathrm{A}} - U_\alpha^{\mathrm{DNS}})}{\max_\alpha(|U_\alpha^{\mathrm{DNS}}|)} \tag{41}$$

and the relative error in the change in the energy in the subdomain $\Omega^{\mathrm{A}}/\Omega^{\mathrm{B}}$ be defined as

$$e^U = \frac{1}{n^{\mathrm{AB}}}\sqrt{\sum_{\alpha\in\mathscr{S}^{\mathrm{AB}}}(e_\alpha^U)^2} \tag{42}$$

where $n^{\mathrm{AB}}$ is the number of atoms in the set $\mathscr{S}^{\mathrm{AB}}$ and $U_\alpha^{\mathrm{A}}$ is the change in the energy of the atom $\alpha$ computed by the coupled model. $U_\alpha^{\mathrm{DNS}}$ is the change in the energy of the atom $\alpha$ in the DNS, and $\max_\alpha(|U_\alpha^{\mathrm{DNS}}|)$ is the maximum change in the energy of an atom in the DNS.

We also examine the error in the displacements using the relative error in the displacement per atom

$$e_\alpha^{L^2} = \frac{\|\mathbf{u}_\alpha^{\mathrm{A}} - \mathbf{u}_\alpha^{\mathrm{DNS}}\|}{b} \tag{43}$$



DOI: 10.1002/nme

and the relative error in the displacements of the atoms in the subdomain $\Omega^{\mathrm{A}}\backslash\Omega^{\mathrm{B}}$:

$$e^{L^2}=\frac{1}{n^{\mathrm{AB}}}\sqrt{\sum_{\alpha\in\mathscr{S}^{\mathrm{AB}}}(e_\alpha^{L^2})^2} \tag{44}$$

where $\mathbf{u}_\alpha^{\mathrm{DNS}}$ is the displacement of the atom $\alpha$ in the DNS.

The second-generation Tersoff–Brenner REBO potential [42] is used to model the graphene at the atomic scale. Under a small displacement assumption, graphene is isotropic and the elasticity tensor $\mathbf{C}$ is given by

$$C_{ijkl}=\mu(\delta_{ik}\delta_{jl}+\delta_{il}\delta_{jk})+\lambda\delta_{ij}\delta_{kl} \tag{45}$$

where $\mu=5.428\,\mathrm{eV}$ and $\lambda=7.148\,\mathrm{eV}$ are Lamé constants. These constants have been derived for graphene modeled by the Tersoff–Brenner potential [43] by Arroyo and Belytschko [44, 45] and are used in all examples. As discussed in [44], graphene is a crystalline layer; therefore, it is a true two-dimensional material and indices $i$, $j$, $k$ and $l$ range over 1 and 2.

### 6.1. *Edge crack in a graphene sheet*

Consider a $247.18\,\text{Å}\times 208.03\,\text{Å}$ graphene sheet as shown in Figure 3; the origin of the domain is located at the center of the sheet. The sheet is oriented such that the zig-zag direction corresponds to the $x$-axis. A crack is created by deleting the bonds from the atomistic model, which are cut by the line $y=9.5\,\text{Å}$ for $x\in(-123.59, 10\,\text{Å})$. The bottom edge of the domain is fully constrained. Displacement boundary conditions are applied to the top edge: $\bar{u}_x=0.01L_x$ and $\bar{u}_y=0.01L_y$, where $L_x=247.18\,\text{Å}$ and $L_y=208.03\,\text{Å}$.

The domain is discretized by a $21\times 21$ triangular element mesh. We will compare the solution of the combined XFEM-BDM model with that obtained by DNS using a fully atomistic model. Figure 4 shows the domain decompositions and discretization of the combined model; the purely atomistic subdomain, $\Omega^{\mathrm{A}}\backslash\Omega^{\mathrm{B}}$, consists only of the domain of the 18 elements surrounding the crack tip. We set the nodal weights, $w_I^{\mathrm{C}}$, of the nodes of these elements to zero and all other nodal weights to 1. Therefore, the bridging domain consists of the elements immediately surrounding

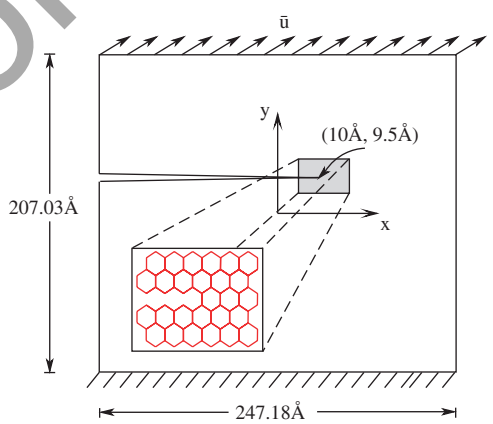


Figure 3. Schematic of the problem of a graphene sheet with an edge crack.





DOI: 10.1002/nme

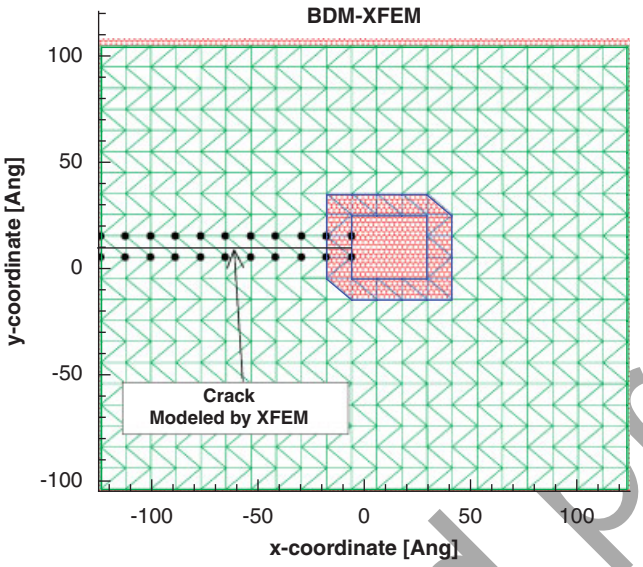


Figure 4. Domain decomposition and discretization of the problem of a graphene sheet with an edge crack for the combined bridging domain method and extended finite element method model. Green and blue lines denote the FEM and the Lagrange multiplier meshes, respectively. Black disks represent the Heaviside-enriched nodes.

the purely atomistic domain and the weight varies linearly from 0 to 1 within one element of the continuum.

In this example the zero contour of the function $\phi(\mathbf{x})$, which defines the location of the crack in the continuum, is given by the problem description: $\phi(\mathbf{x})=0=\{\mathbf{x}|x\in(-123.59, 10\,\text{Å})$ and $y=9.5\,\text{Å}\}$. In general, $\phi(\mathbf{x})$ must be determined from the atomistic displacements, i.e. from the location of the crack in the atomistic model, but in this problem it is straightforward. From $\phi(\mathbf{x})$ the set of Heaviside step function-enriched nodes (those in set $\mathscr{N}^{\phi}$) is determined. These are illustrated by black disks in Figure 4.

We note that most concurrent multiscale models, such as the standard BDM and the quasicontinuum method, require atoms along the entire crack surface. In the combined XFEM-BDM model, we can significantly reduce the number of atoms in the model by modeling a long portion of the crack by a discontinuity in the continuum model. This is accomplished by only 44 continuum-enriched degrees of freedom. The enrichment of the continuum elements in the bridging domain allows cracks to pass from the atomistic model to the continuum model.

Figure 5 shows the relative errors per atom from the combined XFEM-BDM model with respect to the DNS for atoms in $\Omega^{\mathrm{A}}\backslash\Omega^{\mathrm{B}}$. The maximum relative error in the change in the energy per atom is $5.5\times10^{-2}$ and occurs at the crack tip, while the maximum relative error in the displacement of an atom is $7.8\times10^{-2}$ and occurs at the bridging domain boundary. The error in the energy is highly localized, while that in the displacements is more diffusive. The relative errors in the change in the energy and in the displacements of atoms in $\Omega^{\mathrm{A}}\backslash\Omega^{\mathrm{B}}$ are $3.6\times10^{-4}$ and $4.2\times10^{-3}$, respectively. The displacement errors tend to localize at the coupling domain boundary likely because of ghost forces from the coupling constraint and because the strains in the continuum model are highest in





DOI: 10.1002/nme

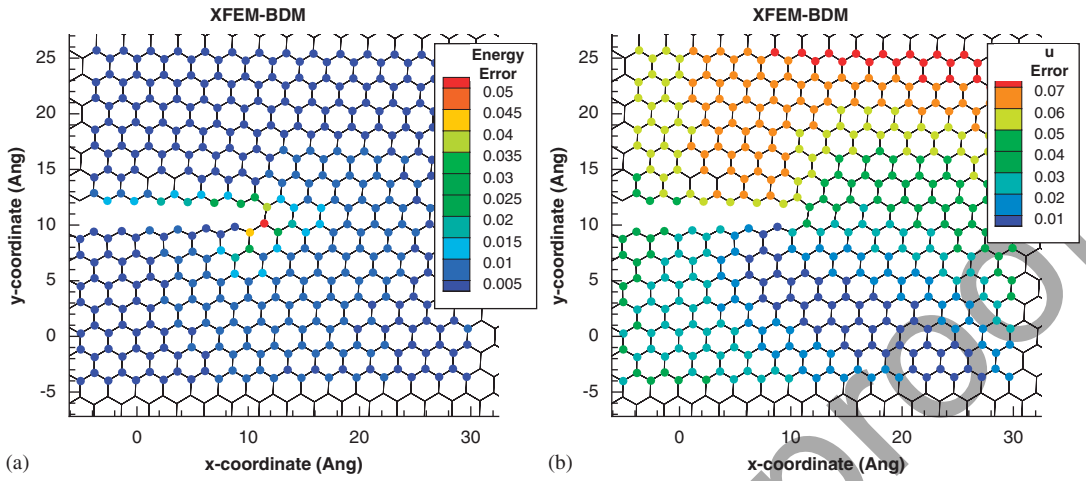


Figure 5. Relative errors per atom of atoms in $\Omega^{A}\backslash\Omega^{B}$ of the combined extended finite element method and bridging domain method model: (a) relative error in the change in the energy per atom and (b) relative error in the displacement per atom.

the coupling domain and so the errors induced by assuming that the continuum is linear elastic and isotropic are largest there. Other sources of error in the model come from free surface effects not captured by the continuum model. These occur along the vertical edges of the domain and along the crack surfaces. The loss in accuracy from the homogenization of the crack is not significant given the reduction in the number of degrees of freedom—the combined XFEM-BDM model uses only 1254 free atoms compared with the 19 788 atoms used in the DNS.

It is important to use a field approximation of the Lagrange multipliers (a weak constraint) instead of pointwise Lagrange multipliers (a strong constraint). We observed significant surface effects in the simulation results. The bonds near the surface behave very differently from the bulk graphene lattice and tend to significantly relax. A stronger constraint forces the strain in the bonds of the surface atoms to exactly match that in the continuum. Since the correct behavior cannot be captured by the continuum model without a surface model such as that in [33], strong constraints overpredict the energies. This observation was previously reported in the one-dimensional studies in [36, 40] and is related to the conclusion in [41] that the Lagrange multiplier mesh should be at least the size of an RVE.

### 6.2. *Dislocation pair in a two-dimensional graphene sheet*

Consider the $239.80\,\text{Å} \times 237.14\,\text{Å}$ graphene sheet shown in Figure 6. The sheet contains a pair of edge dislocations with the Burgers vector magnitude $b = \|\mathbf{b}\| = 2.46\,\text{Å}$ along the $x$-axis. In this example, the slip plane of the dislocation dipole is parallel to the $x$-axis and is offset from the $x$-axis by 1 Å. The cores are separated by a distance of $65b$. Pure shear displacement boundary conditions are applied to all edges of the domain such that $\bar{u}_x = 0.01y$ and $\bar{u}_y = 0.01x$.

Mechanisms for dislocation creation and motion in graphene have been described in [46]. The 5-7-7-5 Stone–Wales defect shown in Figure 7 can be viewed as a pair of edge dislocations; Stone–Wales defects can be created in a perfect lattice by bond rotation (the evolution from state





DOI: 10.1002/nme

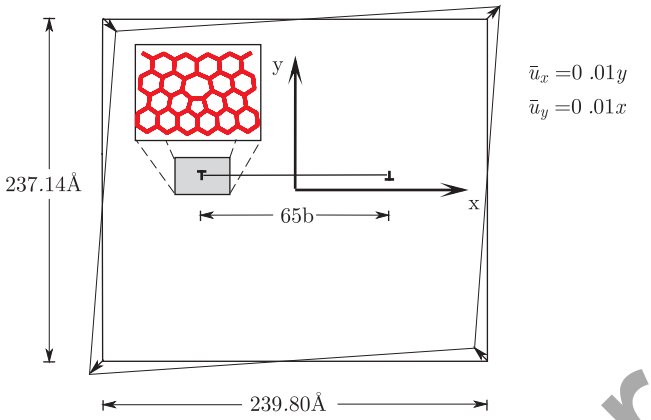


Figure 6. Schematic of the problem of a graphene sheet with a pair of edge dislocations.

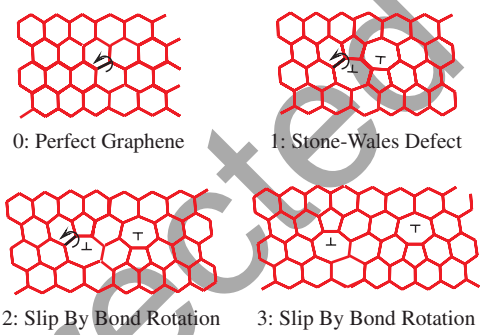


Figure 7. Illustration of the mechanism for the formation and propagation of edge dislocations in graphene. State 0 illustrates pristine graphene and state 1 illustrates a 5-7-7-5 Stone–Wales defect. State 2 shows a dislocation pair after one bond rotation and state 3 shows a dislocation pair after two bond rotations.

0 to 1). Dislocation motion occurs by bond rotation of the bond of a seven atom ring, which is adjacent to a five atom ring (the evolution of state 1 to 2 and state 2 to 3).

We explicitly create the dislocation pair by rotating bonds that are cut by the line $y=1$, for $x \in (-32.5b, 32.5b)$. As was the case for modeling cracks, the location of the zero contour of the function $\psi(\mathbf{x})$, which defines the portion of the glide plane, is known: $\psi(\mathbf{x})=0=\{\mathbf{x}|y=1\,\text{Å}$ and $x \in (-32.5b, 32.5b)\}$. Since in this example we know which slip system is activated, we also know the magnitude and direction of the Burgers vector away from the dislocation core. A method for extracting equivalent continuum discontinuities from atomistic displacements is not trivial. Extracting these discontinuities for dislocations from the atomistic displacements will not be straightforward, but knowledge about preferred slip systems limits the number of potential equivalent continuum discontinuities.

We will compare the solutions of both a standard BDM model and a combined XFEM-BDM model to further demonstrate the advantage of adopting an XFEM approximation in the continuum.



DOI: 10.1002/nme

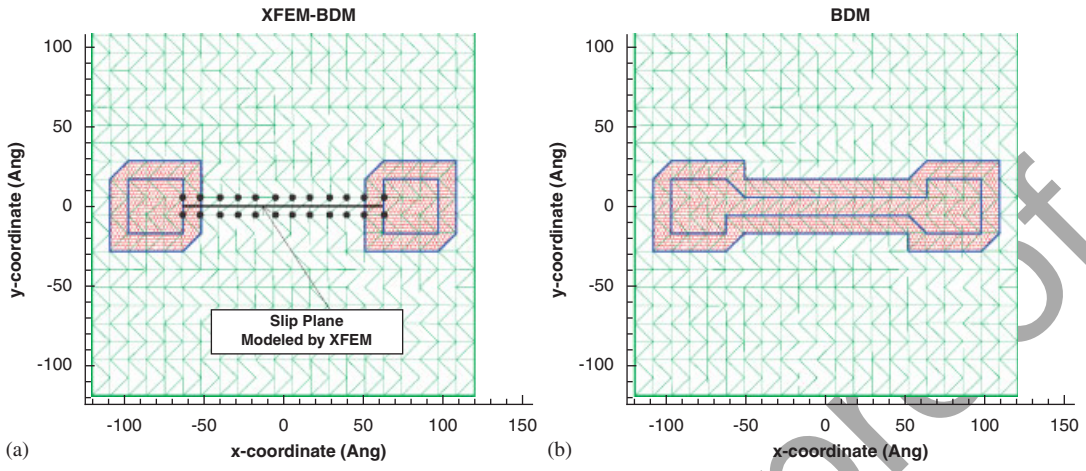


Figure 8. Domain decomposition of the problem of a graphene sheet with a pair of edge dislocations: (a) combined extended finite element and bridging domain method model and (b) standard bridging domain method model. Green and blue lines denote the FEM and the Lagrange multiplier meshes, respectively. Black disks represent the nodes enriched by the dislocation enrichment function.

The discretization and domain decomposition of the problem for both methodologies is shown in Figure 8. In both models, the continuum is discretized by a $21\times21$ triangular element mesh. The coupling domain is taken as a single layer of elements and the Lagrange multiplier mesh is chosen to coincide with the FE mesh. In the standard BDM model, the atomistic domain must consist of the regions surrounding the dislocation cores and the glide plane between the two cores. In the combined XFEM-BDM model, the atomistic domain consists only of the regions surrounding the dislocation cores. Figure 8(a) also illustrates the enriched nodes (those in set $\mathcal{N}^{\psi}$) required to introduce the discontinuity due to slip along the glide plane. We note that in contrast to the crack example, the enrichment for the dislocation does not introduce any additional unknowns. The effect of the dislocation enrichment appears as a force on the right-hand side of the system equations, see Equation (38). The fully atomistic DNS, the standard BDM model and the combined XFEM-BDM model contain 21 534, 3652 and 2308 unconstrained atoms, respectively.

Figure 9 shows the relative error in the change in the energy per atom, with respect to the DNS, of atoms near the right-hand side dislocation core obtained from the standard BDM model and the combined XFEM-BDM model. Atoms are shown in the deformed configuration. We observe that the displacements of the two models are indistinguishable and that the magnitude and distribution of the relative error is very similar for both models. This is also reflected by the relative errors in the energy of the fully atomistic domain around the defect, which are $3.7\times10^{-5}$ and $4.1\times10^{-5}$ for the standard BDM and the XFEM-BDM models, respectively. The relative error in the displacements is $1.0\times10^{-3}$ for both the standard BDM and the combined XFEM-BDM models. We noticed that the errors in the combined XFEM-BDM are largely due to shortcomings in the standard BDM such as the linear constitutive model and ghost forces from the coupling constraint and not from the XFEM model of slip in the continuum. The relative errors in this example are less than those in the previous example in part because there are no free surface effects since the entire domain boundary is constrained.





DOI: 10.1002/nme

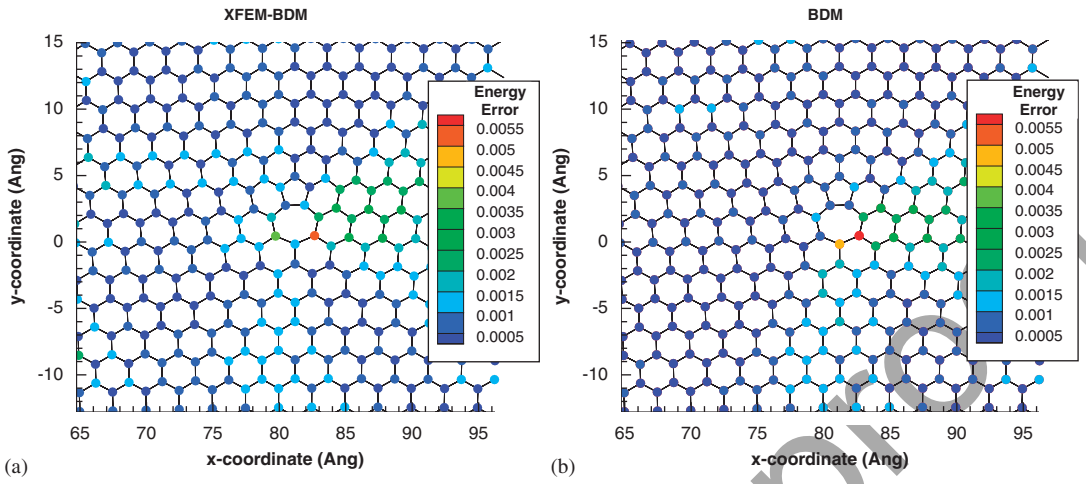


Figure 9. Relative error in the change in the energy per atom of atoms near the rightmost dislocation core in the problem of a graphene sheet with a pair of edge dislocations: (a) combined extended finite element and bridging domain method model and (b) standard bridging domain method model.

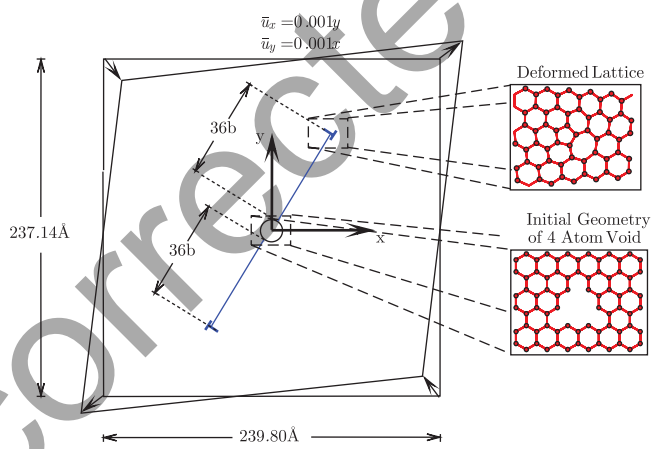


Figure 10. Schematic of the problem of a graphene sheet with a four atom void and a pair of edge dislocations.

### 6.3. *Dislocation emitted from a void in a graphene sheet*

Consider a 239.80 Å × 237.14 Å graphene sheet as shown in Figure 10. In the center of the domain is a four atom void from which two dislocations have been emitted at angles of 60 and 240° with respect to the positive $x$-axis. Each dislocation travels a distance of $36b$ from the void. The problem solved here is to find the final equilibrium configuration and energy under shear. Pure shear displacement boundary conditions are applied to all edges of the domain such that $\bar{u}_x = 0.001y$



DOI: 10.1002/nme

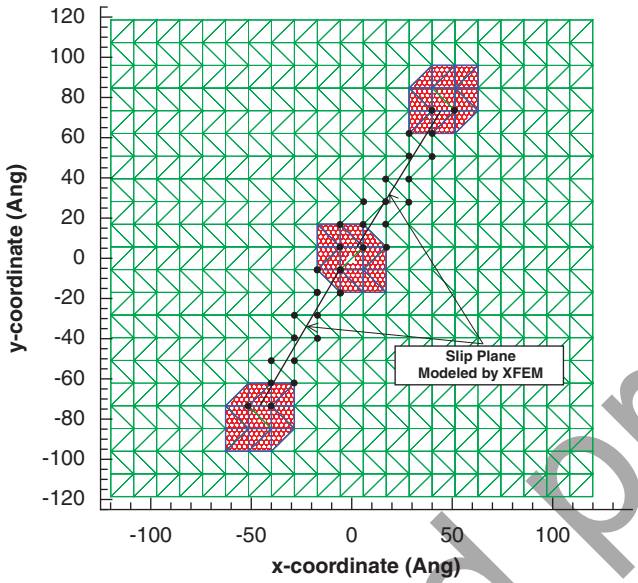


Figure 11. Domain decomposition of the problem of two dislocations emitted from a void for the combined extended finite element method and bridging domain method model. Green and blue lines denote the FEM and the Lagrange multiplier meshes, respectively. Black disks represent the nodes enriched by the dislocation enrichment function.

and $\bar{u}_y = 0.001x$. As in the previous example, the location of the slip plane is known in advance, as is the magnitude and direction of the Burgers vector: $\mathbf{b} = (b\cos(\pi/3), b\sin(\pi/3))$ and $b = 2.46\,\text{Å}$.

The discretization and domain decomposition of the problem for the combined XFEM-BDM model is shown in Figure 11. The continuum is discretized by a $21 \times 21$ triangular element mesh. The coupling domain is taken as a single layer of elements and the Lagrange multiplier mesh is chosen to coincide with the FE mesh. In the combined model, the atomistic domain consists only of the region surrounding the void and the dislocation cores. Figure 11 also illustrates the enriched nodes (those in set $\mathcal{N}^{\psi}$) required to introduce the discontinuity due to slip along the glide plane into the continuum model. Note that in this model, the glide plane is not parallel to any element edges; therefore, modeling the glide plane by releasing nodes would not be possible and consequently XFEM becomes advantageous. The combined model has only 1188 atoms, while the full DNS has 21 530 atoms.

Figure 12 shows the relative error in the change in the energy per atom of the combined XFEM-BDM model with respect to the DNS. The maximum relative error in energy per atom occurs at the edge of the bridging domain. The maximum displacement error per atom also occurs near the bridging domain boundary. The relative errors in the change in the energy and in the displacements are $2.1 \times 10^{-4}$ and $8.4 \times 10^{-4}$, respectively. This is quite good given the proximity of the continuum domain to the core and the coarseness of the continuum mesh. This example clearly shows that the adoption of the XFEM approximation results in a significant reduction in the number of atoms in the model, without a significant loss of accuracy at the dislocation core.





DOI: 10.1002/nme

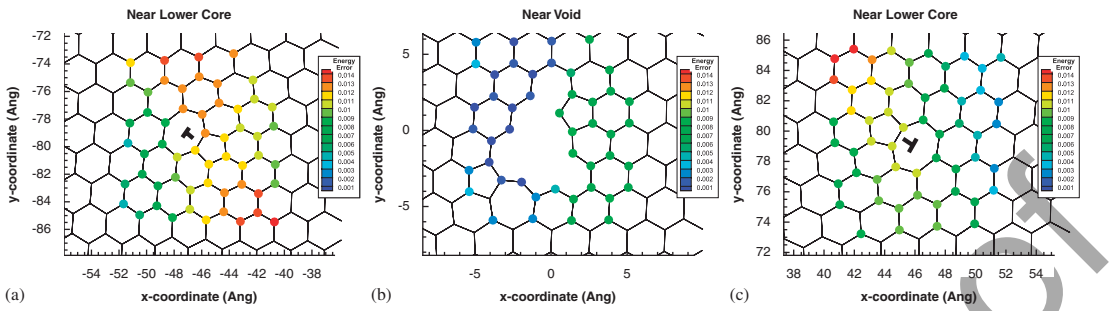


Figure 12. Relative error in the change in the energy per atom of atoms in the fully atomistic domain for the problem of a pair of dislocations emitted from a void: (a) atoms in the fully atomistic domain near the lower dislocation core; (b) atoms in the fully atomistic domain near the void; and (c) atoms in the fully atomistic domain near the upper dislocation core.

Table I. Summary of relative errors of each example for the combined XFEM-BDM model with respect to fully atomistic direct numerical simulations.

| Problems | $\max_\alpha(e_\alpha^U)$ | $e^U$ | $e^{L^2}$ | No. atoms XFEM-BDM | No. atoms DNS |
|---|---|---|---|---|---|
| Edge crack | $5.6\times10^{-2}$ | $4.2\times10^{-3}$ | $3.6\times10^{-4}$ | 1254 | 19788 |
| Dislocation pair | $5.9\times10^{-3}$ | $1.0\times10^{-3}$ | $4.1\times10^{-5}$ | 2308 | 21534 |
| Dislocation pair and void | $1.3\times10^{-2}$ | $8.4\times10^{-4}$ | $2.1\times10^{-4}$ | 1188 | 21530 |

The errors in the energy (both local and in the fully atomistic region) and in the displacement compared to fully atomistic models (DNS) for the three problems are summarized in Table I along with the number of atoms in the coupled XFEM-BDM and DNS models.

## 7. CONCLUSIONS

We have developed a concurrent multiscale method for coupling atomistics and continua when the deformations at the continuum level corresponding to the atomistic phenomena are discontinuous, i.e. in the presence of dislocations and cracks. The framework is based on the Bridging Domain Method (BDM), where compatibility between overlapping continuum and atomistic domains is enforced by Lagrange multipliers. The key contribution of this paper is the coupling of the Extended Finite Element Method (XFEM) with the atomistic model. This allows for discontinuities in the atomistic domain to be effectively passed into the continuum domain.

In the examples considered here, atomistic models of the material behavior of graphene were used in the region near crack tips and dislocation cores, whereas a continuum model is adopted in the rest of the domain. The discontinuity due to a crack is incorporated into the continuum model by the enrichment of the standard FEM approximation by the Heaviside step function. Similarly, slip across the glide plane in the continuum domain is modeled by a tangential step function enrichment.





DOI: 10.1002/nme

We have studied several examples of defected two-dimensional graphene: an edge crack under mixed mode loading, a pair of edge dislocations under shear loading and a pair of edge dislocations emitted from a void under shear loading. Simulations using the combined bridging domain method and extended finite element method (XFEM-BDM) have been compared with direct numerical simulations (DNS) by fully atomistic models. The relative errors in the change in the energy in the region around the defects with respect to the DNS were $3.6\times10^{-4}$, $4.1\times10^{-5}$ and $2.1\times10^{-4}$, respectively. The relative errors in the displacements with respect to the DNS were $4.2\times10^{-3}$, $1.0\times10^{-3}$ and $8.4\times10^{-4}$, respectively. The local per atom errors in displacements are the largest near the coupling domain. This suggests that the errors in the combined model are largely due to the assumption of linear isotropic behavior of the continuum and ghost forces from the coupling constraint and so are not due to the replacement of the atomistic discontinuity by a discontinuity in the continuum model. The continuum model in the XFEM-BDM model can be easily extended to a non-linear hyperelastic constitutive model based on a Cauchy–Born approximation. In the problems solved, which involve relatively small discontinuities, the combined XFEM-BDM models used about 15 times fewer atoms than the fully atomistic model and so the accuracy of the combined XFEM-BDM models is quite acceptable.

The performance of the combined XFEM-BDM model of the edge dislocation problem compares well with a standard BDM model of the same problem. In the standard BDM, all slips had to be modeled by the atomistic model. The accuracy of the two models is similar even though the XFEM-BDM model uses about 50% fewer atoms. When compared with DNS, the two models yield global and local errors in energies and displacements which are very similar. The magnitude and distribution of the local relative errors in the change in the energy per atom is also similar. This substantiates the conclusion that the errors in the combined model are largely due to shortcomings in the standard BDM and are not due to the replacement of the atomistic discontinuity by a discontinuous continuum model.

In the future we will aim to make this new framework adaptive so that as cracks and dislocations propagate, the regions ahead of the crack tips and cores will be converted from continuum to atomistics and the discontinuities in the atomistic domain behind the tips and cores will be coarsegrained. Determining an equivalent continuum crack from the atomistic displacements was straightforward in the problem solved here; however, for more complex curved cracks, this could be an issue that demands significant care. Determining the equivalent continuum dislocation slip from the atomistic discontinuity will likely be easier since for a given crystal the location of potential slip systems is known and the Burgers vector is well defined away from the cores. Still, determining the correct discontinuity from among all possibilities in a computationally efficient way may not be trivial.

In traditional concurrent multiscale simulations, discontinuities from cracks and dislocation slip must be represented by the atomistic model. In contrast, the new method described here allows large portions of these discontinuities to be represented by a continuum. Therefore, a significant reduction in the number of atomistic degrees of freedom is possible. Furthermore, the numerical examples presented here show that this can be accomplished without compromising atomistic resolution and accuracy in the near crack tip or dislocation core regions.

ACKNOWLEDGEMENTS

We gratefully acknowledge the support of the Army Research Office under grants W911NF-05-1-0049 and W911NF-08-1-0212.



DOI: 10.1002/nme

## REFERENCES


1. Abraham FF, Broughton JQ, Bernstein N, Kaxiras E. Spanning the continuum to quantum length scales in a dynamic simulation of brittle fracture. *Europhysics Letters* 1998; **44**(6):783–787.
2. Khare R, Mielke SL, Paci JT, Zhang S, Ballarini R, Schatz GC, Belytschko T. Coupled quantum mechanical/molecular mechanical modeling of the fracture of defective carbon nanotubes and graphene sheets. *Physical Review B* 2007; **75**(7):75412.
3. Oden JT, Prudhomme S, Romkes A, Bauman PT. Multiscale modeling of physical phenomena: adaptive control of models. *SIAM Journal on Scientific Computing* 2006; **28**(6):2359.
4. Curtin WA, Miller RE. Atomistic/continuum coupling in computational material science. *Modelling and Simulation in Materials Science and Engineering* 2003; **11**:R33–R68.
5. de Pablo JJ, Curtin WA. Multiscale modeling in advanced materials research: challenges, novel methods, and emerging applications. *MRS Bulletin* 2007; **32**:905–911.
6. Liu WK, Jun S, Qian D. Computational nanomechanics of materials. *Journal of Computational and Theoretical Nanoscience* 2008; **5**(5):970.
7. Tadmor EB, Ortiz M, Philips R. Quasicontinuum analysis of defects in solids. *Philosophical Magazine A* 1996; **73**(6):1529–1563.
8. Rodney D, Phillips R. Structure and strength of dislocation junctions: an atomic level analysis. *Physical Review Letters* 1999; **82**(8):1704–1707.
9. Fago M, Hayes RL, Carter EA, Ortiz M. Density-functional-theory-based local quasicontinuum method: prediction of dislocation nucleation. *Physical Review B* 2004; **70**(10):100102.
10. Shilkrot LE, Curtin WA, Miller RE. A coupled atomistic/continuum model of defects in solids. *Journal of the Mechanics and Physics of Solids* 2002; **50**(10):2085–2105.
11. Shilkrot LE, Miller RE, Curtin WA. Multiscale plasticity modeling: coupled atomistics and discrete dislocation mechanics. *Journal of the Mechanics and Physics of Solids* 2004; **52**(4):755–787.
12. van der Giessen E, Needleman A. Discrete dislocation plasticity: a simple planar model. *Modelling and Simulation in Materials Science and Engineering* 1995; **3**:689–735.
13. Belytschko T, Xiao SP. Coupling methods for continuum model with molecular model. *International Journal for Multiscale Computational Engineering* 2003; **1**(1):115–126.
14. Xiao SP, Belytschko T. A bridging domain method for coupling continua with molecular dynamics. *Computer Methods in Applied Mechanics and Engineering* 2004; **193**:1645–1669.
15. Zhang S, Mielke SL, Khare R, Troya D, Ruoff RS, Schatz GC, Belytschko T. Mechanics of defects in carbon nanotubes: atomistic and multiscale simulations. *Physical Review B* 2005; **71**:115403.
16. Zhang S, Khare R, Lu Q, Belytschko T. A bridging domain and strain computation method for coupled atomistic–continuum modelling of solids. *International Journal for Numerical Methods in Engineering* 2007; **70**:913–933.
17. Belytschko T, Black T. Elastic crack growth in finite elements with minimal remeshing. *International Journal for Numerical Methods in Engineering* 1999; **45**:601–620.
18. Moës N, Dolbow J, Belytschko T. A finite element method for crack growth without remeshing. *International Journal for Numerical Methods in Engineering* 1999; **46**:131–150.
19. Gracie R, Belytschko T. An extended bridging domain method for continuum–atomistic simulations of discontinuities. *World Congress on Computation Mechanics*, Venice, July 2008.
20. Aubertin P, de Borst R, Réthoré J. Atomistic–continuum coupling for dynamic crack propagation. *World Congress on Computation Mechanics*, Venice, July 2008.
21. Melenk JM, Babuška I. The partition of unity finite element method: basic theory and applications. *Computer Methods in Applied Mechanics and Engineering* 1996; **139**:290–314.
22. Ventura G, Moran B, Belytschko T. Dislocations by partition of unity. *International Journal for Numerical Methods in Engineering* 2005; **62**(11):1463–1487.
23. Gracie R, Ventura G, Belytschko T. A new fast method for dislocations based on interior discontinuities. *International Journal for Numerical Methods in Engineering* 2007; **69**:423–441.
24. Gracie R, Oswald J, Belytschko T. On a new extended finite element method for dislocations: core enrichments. *Journal of the Mechanics and Physics of Solids* 2008; **56**:200–214. DOI: 10.1016/j.jmps.2007.07.010.
25. Simone A, Duarte CA, Van der Giessen E. A generalized finite element method for polycrystals with discontinuous grain boundaries. *International Journal for Numerical Methods in Engineering* 2006; **67**:1122–1145.




DOI: 10.1002/nme

26. Fish J, Nuggehally MA, Shephard MS, Picu CR, Badia S, Parks ML, Gunzburger M. Concurrent AtC coupling based on a blend of the continuum stress and the atomistic force. *Computer Methods in Applied Mechanics and Engineering* 2007; **196**(45–48):4548–4560.
27. Ben Dhia H, Rateau G. The Arlequin method as a flexible engineering design tool. *International Journal for Numerical Methods in Engineering* 2005; **62**:1442–1462.
28. Badia S, Bochev P, Fish J, Gunzburger M, Lehoucq R, Nuggehally M, Parks ML. A force-based blending model for atomistic-to-continuum coupling. *International Journal for Multiscale Computational Engineering* 2005; **5**(5):369–386.
29. Li Z, Dharap P, Sharma P, Nagarajaiah S, Yakobson BI. Continuum field model of defect formation in carbon nanotubes. *Journal of Applied Physics* 2005; **97**:074303.
30. Oswald J, Gracie R, Khare R, Belytschko T. An extended finite element method for dislocations in complex geometries: thin films and nanotubes. *Computer Methods in Applied Mechanics and Engineering*, in press.
31. Belytschko T, Loehnert S, Song JH. Multiscale aggregating discontinuities: a method for circumventing loss of material stability. *International Journal for Numerical Methods in Engineering* 2008; **73**:869–894.
32. Arroyo M, Belytschko T. An atomistic-based finite deformation membrane for single layer crystalline films. *Journal of the Mechanics and Physics of Solids* 2002; **50**(9):1941–1977.
33. Park H, Klein P, Wagner G. A surface Cauchy–Born model for nanoscale materials. *International Journal for Numerical Methods in Engineering* 2006; **68**:1072–1095.
34. Liu X, Li S. A cohesive finite element for quasi-continua. *Computational Mechanics* 2008; **42**(4):543–553.
35. Fish J. Hierarchical modelling of discontinuous fields. *Communications in Applied Numerical Methods* 1992; **8**(7):443–453.
36. Guidault PA, Belytschko T. On the $L^2$ and the $H^1$ couplings for an overlapping domain decomposition method using Lagrange multipliers. *International Journal for Numerical Methods in Engineering* 2007; **70**:322–350.
37. Bauman PT, Ben Dhia H, Elkhodja N, Oden JT, Prudhomme S. On the application of the Arlequin method to the coupling of particle and continuum models. *Computational Mechanics* 2008; **42**(4):511–530.
38. Xu M, Belytschko T. Conservation properties of the bridging domain method for coupled molecular/continuum dynamics. *International Journal for Numerical Methods in Engineering* 2008; **76**(3). DOI: 10.1002/nme.2323.
39. Liu DC, Nocedal J. On the limited memory bfgs method for large scale optimization. *Mathematical Programming* 1989; **45**(1):503–528.
40. Guidault PA, Belytschko T. Bridging domain methods for coupled atomistic–continuum models with $L^2$ or $H^1$ couplings. *International Journal for Numerical Methods in Engineering*, DOI: 10.1002/nme.2481.
41. Prudhomme S, Ben Dhia H, Bauman PT, Elkhodja N, Oden JT. Computational analysis of modeling error for the coupling of particle and continuum models by the Arlequin method. *Computer Methods in Applied Mechanics and Engineering*, DOI: 10.1016/j.cma.2008.03.014.
42. Brenner DW, Shenderova OA, Harrison JA, Stuart SJ, Ni B, Sinnott SB. A second-generation reactive empirical bond order (rebo) potential energy expression for hydrocarbons. *Journal of Physics*: *Condensed Matter* 2002; **14**(4):783–802.
43. Brenner DW. Empirical potential for hydrocarbons for use in simulating the chemical vapor deposition of diamond films. *Physical Review B* 1990; **42**(15):9458–9471.
44. Arroyo M, Belytschko T. Finite element methods for the non-linear mechanics of crystalline sheets and nanotubes. *International Journal for Numerical Methods in Engineering* 2004; **59**:419–456.
45. Arroyo M, Belytschko T. Finite crystal elasticity of carbon nanotubes based on the exponential Cauchy–Born rule. *Physical Review B* 2004; **69**(11):115415.
46. Nardelli MB, Yakobson BI, Bernholc J. Mechanisms of strain release in carbon nanotubes. *Physical Review B* 1998; **57**:R4277–R4280.






DOI: 10.1002/nme